(Preprint) AAS 17-483

ELECTROSTATICALLY CHARGED SPACECRAFT FORMATION ESTIMATION USING LINEARIZED RELATIVE ORBIT ELEMENTS

Trevor Bennett* **and Hanspeter Schaub†**

Touchless methods of actuating and detumbling large Earth-orbiting objects are of increasing importance to active satellite servicing and debris mitigation strategies. Electrostatic detumble, the process of using electrostatic interaction between two spacecraft, is able to touchlessly detumble large targets in Geostationary orbit. This is of interest for reducing tumble rates of several degrees per second down to rates conducive to capture and servicing. The effectiveness of the electrostatic detumble control is dependent upon the electrostatic potential of both craft and the relative separation. This study develops the estimation approach to obtain the electrostatic potential of the target object using only relative motion measurements. The sensitivity to electrostatic perturbations are developed using the Linearized Relative Orbit Elements relative motion description. The analytical conclusions are validated using a two-time-scale Kalman filter numerical simulation.

INTRODUCTION

On-orbit satellite servicing and orbital debris removal are increasingly important to both governmental and commercial interests. In particular, the Geostationary orbit (GEO) is one of the most valuable Earth orbiting regions requiring operators to maintain tight orbital slots and adhere to end-of-life practices to protect assets insured over 13 Billion US dollars.[1] The Geostationary belt is therefore a prime candidate for improved satellite servicing and removal strategies. Many mechanical, tether, and net-based systems have been considered for interfacing with the on-orbit target.[2–4] However, the target object may tumble at rates of up to 10's of degrees per second inhibiting conventional grappling techniques.[5,6] Touchless methods that avoid the inherent collision risk or fuel-expensive relative motion, such as electrostatic actuation and Ion Shepherd, have been proposed for on-orbit attitude control of spacecraft.

Electrostatic actuation of spacecraft has been explored as early as the 1960s developing both the understanding of charging dynamics and electrostatic control for Earth-orbiting satellites.[7–13] In addition, electrostatic actuation with a passive object is being considered for both large GEO debris mitigation[14–17] as well as touchless asteroid spin control.[18,19] Electrostatic actuation my also be used for target re/de-orbiting or even electrostatic formation flying.[17,20] Specifically, Reference 21 shows that the Geostationary Orbit environment is a prime candidate region where space plasma conditions enable electrostatic interactions across 10's to 100's of meters maintained with only Watt-levels of power. The electrostatic detumble concept, which requires no direct contact, is shown in Figure 1.

*Graduate Research Assistant and NSTRF Fellow, Aerospace Engineering Sciences, University of Colorado.

†Alfred T. and Betty E. Look Professor of Engineering, Associate Chair of Graduate Affairs, Department of Aerospace Engineering Sciences, University of Colorado, 431 UCB, Colorado Center for Astrodynamics Research, Boulder, CO 80309-0431

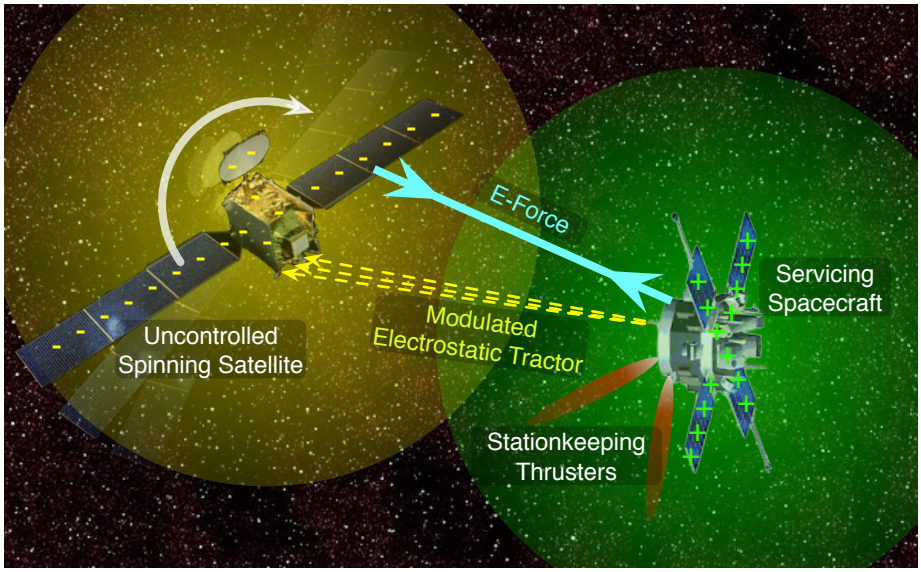

Figure 1. Electrostatic actuation technology enabling diverse service mission profiles.

Knowledge of the electrostatic potential is required for electrostatic tug and electrostatic detumble mission concepts. Several modeling approaches have been considered for specific applications. The electrostatic interaction between the two craft is modeled in the relative navigation and control by the Multi-Sphere Method (MSM) as a faster than real time lumped-charge approach.[22] This method utilizes the position-dependent capacitance to compute the local charging on a spacecraft with knowledge of the spacecraft potential and therefore assumes constant potentials on the target craft. While the MSM model provides high accuracy modeling of the charge movement within a spacecraft, the electrostatic potential is a non-stationary process achieved by the charge transfer of the servicing spacecraft and coupled with the space plasma. Some work has been done to compute the target spacecraft potential through modeling the space plasma interaction.[23] Modeling the space plasma requires information regarding the current sources on and off of the spacecraft which has posed a challenge for modeling even the potential on a controlled spacecraft.[31–33] Electrostatic tug studies, which require knowledge of the target craft potential as well, have developed electrostatic potential modeling as a flow of charge transfer and external sources.[23] Such studies are sensitive to the modeling of the space environment. Additional research has explored the estimation of the target potential from Langmuir probe placement without modeling the charge transfer process.[?] There is an opportunity to combine the electrostatic modeling provided by MSM and plasma interaction with the measurements from relative states to best estimate the necessary target craft potential.

Of particular interest is whether the target spacecraft potential may be obtained from relative motion observations rather than space plasma measurements. Consider the formation flight of two electrostatically charged spacecraft as shown in Figure 2. The relative position of these two craft may be represented by a variety of relative motion parameters. However, Reference 24 introduced Linearized Relative Orbit Elements (LROE) as an effective element set for circular chief formation flying guidance and control. The LROE relative motion description has been applied to the electrostatic detumble study, and other touchless line-of-sight methods, by enabling guidance optimization and feedback control for proximity operations.[25] It was also shown that the relative motion could be estimated using the LROE state set.[26] The LROE relative motion description is utilized to describe

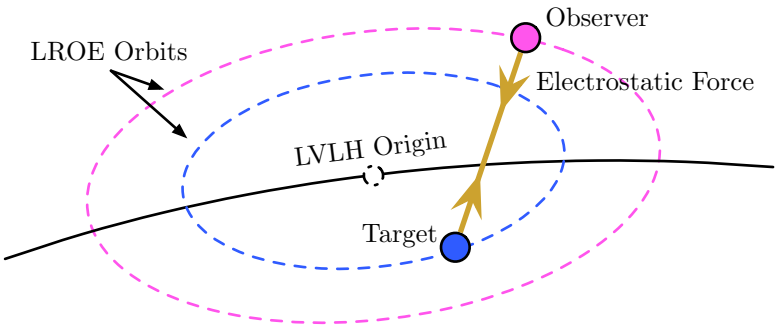

Figure 2. Relative positions of the observer and target as described by LROEs.

both the target and servicer spacecraft using a reference LVLH point to remain consistent with the circular chief assumption.

The electrostatic interaction between the two craft perturbs both spacecraft from nominal relative orbits. The electrostatic interaction is modeled using MSM and the perturbation accelerations are incorporated into the kinematic equations for LROEs. The present challenge is to determine if changes in the relative motion are sufficient to touchlessly obtain the charging behavior of the target craft. The servicing craft is assumed to take bearings and range measurements of the target and focuses sufficient electron, or ion, beam current to charge the target craft. This study develops the line-of-sight measurement sensitivity to a perturbation force for particular relative orbit geometries. This study demonstrates the estimation of the electrostatic potential through Kalman filter numerical simulations. The resulting relative orbit conclusions will inform the electrostatic system identification during proximity operations.

REVIEW OF ELECTROSTATIC FORCE/TORQUE MODELING

The electrostatic interaction between two craft is accurately approximated for faster than real time control and simulation applications by the The Multi-Sphere Method (MSM). MSM represents the spacecraft electrostatic charging model as a collection of spherical conductors carefully dispersed through the body.[22] The validated MSM model is used in faster-than-real-time simulations and control developments where the sphere-to-sphere electrostatic forces are determined by the charges residing on each sphere. The time-varying charges are computed from the prescribed electric potentials according to the self and mutual capacitance relationships in Eq. (1), where $k_c = 8.99 \times 10^9$ N·m^2/C^2 and q_i is the charge of each sphere.[27,28]

$$\phi_i = k_c \frac{q_i}{R_i} + \sum_{j=1, j\neq i}^{m} k_c \frac{q_j}{r_{i,j}} \tag{1}$$

The term R_i denotes the radius of the i^{th} conducting sphere and $r_{i,j}$ denotes the vector between the i^{th} and j^{th} conducting spheres. These relations can be collected in matrix form.

$$\begin{bmatrix} \phi_1 \\ \phi_2 \end{bmatrix} = k_c \begin{bmatrix} 1/R_1 & 1/r_{1,2} \\ 1/r_{1,2} & 1/R_2 \end{bmatrix} \begin{bmatrix} q_1 \\ q_2 \end{bmatrix} \tag{2}$$

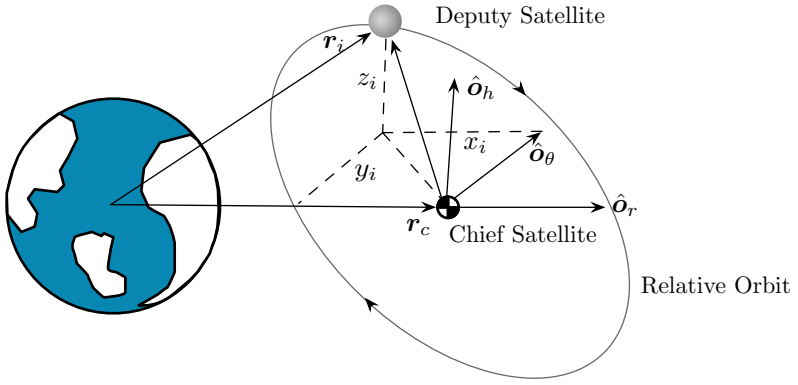

Figure 3. Local vertical local horizontal rotating Hill frame for formation flying.

Inverting the elastance matrix multiplying the charge at a given instant in time produces the forces on the respective spacecraft given by the summations[27]

$$\boldsymbol{F}_2 = k_c q_1 \sum_{i=a}^{c} \frac{q_i}{r_i^3} \boldsymbol{r}_i \tag{3}$$

The use of Eq. (3) enables the electrostatic interaction to be computed at each simulation time step. The electrostatic force is the perturbing acceleration for the two spacecraft system. The following section describes the Linearized Relative Orbit Elements that capture the relative motion effect when a perturbation acceleration is applied.

OVERVIEW OF THE NONSINGULAR LROE SET

The relative motion of two satellites can be described by the inertial state vector difference in the deputy, or target, and chief. This study is most concerned with the relative motion described in a local coordinate frame. Consider the Hill frame defined in Figure 3.[29] The Clohessy-Wiltshire relative orbit equations can be derived from the Cartesian coordinates shown in Figure 3.[30] A slight modification to the CW equations removes the α and β ambiguity and largely preserves the inherent insight.[24] The ambiguity of the linear combination of A_0 and α, or B_0 and β, is removed in place of two perpendicular scaling terms. The modified non-singular LROE set therefore becomes

$$x(t) = A_1 \cos(nt) - A_2 \sin(nt) + x_{\text{off}} \tag{4a}$$

$$y(t) = -2A_1 \sin(nt) - 2A_2 \cos(nt) - \frac{3}{2} nt x_{\text{off}} + y_{\text{off}} \tag{4b}$$

$$z(t) = B_1 \cos(nt) - B_2 \sin(nt) \tag{4c}$$

The LROE state provides the relative motion geometry in the absence of perturbations. The nominally invariant nonsingular LROE state vector $\boldsymbol{X}_{\text{NS}}$, is defined as

$$\boldsymbol{S}_{\text{NS}} = (A_1, A_2, x_{\text{off}}, y_{\text{off}}, B_1, B_2) \tag{5}$$

In the presence of perturbations, a Lagrangian Bracket formulation may be used to generate the specific LROE evolution equations.[26] The dynamics of the state vector are required for navigation filter applications. As described, the LROE set is considered to be invariant while the spacecraft pairs are

influenced only by two-body gravitational effects. However, more accuracy to the dynamic modeling and filter applicability requires additional forces or perturbations to drive the LROE evolution. First derived in Reference 26, the dynamics of the LROE state can be obtained by applying Lagrange Brackets to the non-singular LROE equations. This approach is analogous to Lagrange's planetary equations in that the LROE set becomes osculating to match the perturbed relative orbit. The nonsingular state vector in Eq. (5) evolves according to Eq. (6) where $\boldsymbol{a}_d$ is the disturbance acceleration in the Hill frame.[26]

$$\dot{\boldsymbol{S}}_{\text{NS}} = \underbrace{\frac{1}{n}\begin{bmatrix} -\sin(nt) & -2\cos(nt) & 0 \\ -\cos(nt) & 2\sin(nt) & 0 \\ 0 & 2 & 0 \\ -2 & 3nt & 0 \\ 0 & 0 & -\sin(nt) \\ 0 & 0 & -\cos(nt) \end{bmatrix}}_{B(\boldsymbol{X},t)} \begin{bmatrix} a_x \\ a_y \\ a_z \end{bmatrix} \tag{6}$$

Eq. (6) is the variational equation of the non-singular LROE set, and is the relative motion equivalent of Gauss' variational equation for inertial orbital motion. Any perturbation or control accelerations can be applied to propagate the LROE variations. Recall that the CW equations already account for two-body motion, so the differential perturbation accelerations can include drag, solar radiation pressure, and higher order gravity. Furthermore, the form in Eq. (6) is valid for both the rectilinear and curvilinear LROE formulations discussed in this manuscript. The matrix is derived from the CW form that all LROE state vectors utilize. Propagating the nonsingular Cartesian and curvilinear forms differ in the coordinitization of the acceleration vector.

ESTIMATING TARGET SPACECRAFT POTENTIAL FROM RELATIVE MOTION

The estimation of the potential on both craft is critical to the control model for electrostatic actuation between spacecraft. The challenge of modeling the electrostatic potential on an instrumented craft has employed a variety of methods. Most notably, spacecraft potentials have been measured directly using Langmuir probes or from observer craft with spectrometers, or the ground, using interferometer.[31–33] Langmuir probes, spectrometers, and interferometers measurements have estimation accuracies reported between 5-10%.[31–33] Supposing that the potential estimation error could be reduced to on the order of 5%, for potential levels of 20 kV expected for electrostatic actuation, the resulting force errors are non-negligible.

The ultimate objective is to achieve sufficient modeling for control applications. Furthermore, the electrostatic modeling as formulated in MSM, Eq. (3), is a good approximation of the true interaction that reduces the spacecraft charging to a single-potential collection of conductors with accuracies errors less than 1-5% if separation distances are larger that 2 craft radii.[?,22] It is therefore most valuable to an on-orbit servicer to estimate the parameters as modeled in the dynamics while allowing for additional perturbations.

The Two-Time-Scale Extended Kalman Filter

An extended Kalman filter (EKF) is selected for the spacecraft electrostatic potential estimation simulation. The choice of a nonlinear filter enables the nominal LROE set to vary more dramatically and converge given poor, or absent, a priori. Furthermore, the EKF is a widely used filter and can

be illustrative as a benchmark for the implementation of alternate estimation approaches. The filter state must include the desired is the spacecraft potential of the target craft. In addition, the relative motion of the two craft must also be included.

Lastly, it is of interest to include the mass of the target as an uncertain parameter. The proposed filter state is the relative position of both the observer and target relative to the LVLH origin, the mass of the target, and the electrostatic potential of both craft.

$$\boldsymbol{X}_{\text{desired}} = \left[\boldsymbol{S}_{\text{obs}},\ \boldsymbol{S}_{\text{targ}},\ \phi_{\text{obs}},\ \phi_{\text{targ}}\right]^T \tag{7}$$

The inclusion of both an LROE state for each spacecraft is required because the electrostatic force will perturb both craft. A reference LVLH origin is used for the system as shown in Figure 2. However, limiting the observations to relative motion restricts the availability of state information. Using an LROE state set for each spacecraft and noting that the perturbation forces are only relative separation dependent, the proposed estimation filter can use a differenced relative position state. Examination of the LROE relative position in Eq. (4) shows that the relative position in the LVLH frame may be described by differencing the Cartesian state which is equivalent to computing a Cartesian relative position using differential elements.

$$\boldsymbol{\Delta S} = \boldsymbol{S}_{\text{targ}} - \boldsymbol{S}_{\text{obs}} \tag{8}$$

Referencing Eq. (2), only one of the two craft potentials is observable given relative separation observations. Therefore, the proposed filter estimates the differential relative position state and the target potential. The servicer/observer spacecraft may obtain estimates of its own potential through probes or ground-based observations.

$$\boldsymbol{X}_{\text{est}} = \left[\boldsymbol{\Delta S},\ \phi_{\text{targ}}\right]^T \tag{9}$$

Superb estimation of the LROE relative position is possible using short observational arcs.[26] The change in the relative position due to an electrostatic forces perturbation is much slower than the convergence of position-only estimation process. When the target craft potential is included in the rapid measurement updates used for relative position estimation, the extended Kalman filter tends to diverge. The filter divergence is a symptom of weak observability and computational precision. A simple solution for correcting this problem is to use longer propagation steps between measurement updates. However, the longer propagation gaps is less desirable for a servicer craft using the relative position estimate to perform station keeping. Therefore, a two-time-scale filter is proposed. Two-time-scale filters find application in estimation where elements of the dynamical system evolve on different time scales. An insightful example of two-time-scale filters is exhibited by the missile-intercept problem where the target vehicle may change course much faster than the smaller corrections to missile trajectory.[34] The two-time-scale estimation approach is directly applicable to the fast-evolving relative motion and the longer (or slower) observation of the target spacecraft electrostatic potential. Consider a nested set of estimation filters where the fast-estimate of the relative position is in part de-coupled from a longer propagation arc estimation of the proposed state in Eq. (9). The two-time-scale filter is shown in Figure 4.

The inner estimation filter that estimates the relative position, shown at the bottom of Figure 4, represents the fast-time estimation of the position. This estimate is achieved through a consider EKF and provides more frequent position information to the servicer spacecraft. The position estimation utilizes the current estimate of the target spacecraft potential with a consider covariance supplied by

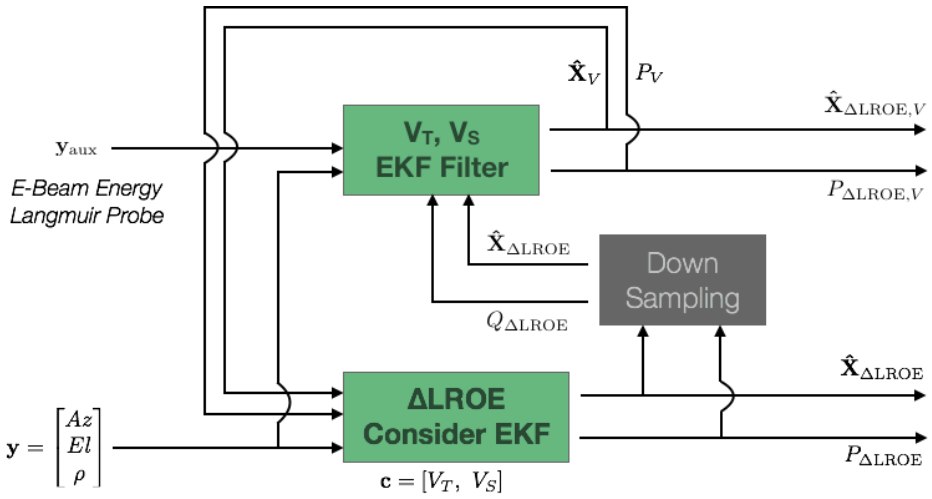

Figure 4. Two-Time-Scale Filter Information Flow

the outer filter. The outer estimation loop estimates the full state in Eq. (9) using the position from the inner loop to propagate the intermediate steps between updates.[34] This ensures that the outer filter computes an estimate on the best available relative position.

The proposed filter utilizes only the bearings and range measurements and assumes a fixed value for the spacecraft potentials. However, given the above approach, additional measurements and filter states may be included in the outer estimation without change to the more rapid relative position updates. The extended Kalman filter formulation used by both inner and outer estimation loops is described in the next section.

Filter Description and Formulation

The LROE filter states are propagated forward in time using Eq. (10) where $\boldsymbol{F}$ are the modeled forcing functions. The dynamics are not constrained to be two-body admitting perturbations in the presented filter formulation. The LROE variational equations, for one state shown in Eq. (6), introduce a time-varying LROE set with filter-modeled electrostatic force perturbation accelerations

$$\dot{\boldsymbol{S}}_k = \boldsymbol{F}(\boldsymbol{X}(t_k), t_k) = B(\boldsymbol{X}(t_k), t_k)\boldsymbol{a}_d \tag{10}$$

where $B(\boldsymbol{X}(t_k), t_k)$ is defined by Eq. (6). The mass is assumed to be constant and electrostatic potentials are assumed to be steady for this study. The state covariance matrix is propagated forward using Eq. (11) requiring the state transition matrix $\Phi\left(t_k, t_{k-1}\right)$ and the addition of process noise $S(t)$.

$$\bar{P}_k = \Phi\left(t_k, t_{k-1}\right) P_{k-1} \Phi^T\left(t_k, t_{k-1}\right) + S_{PN}(t) \tag{11}$$

The process noise matrix S_{PN} is added at every time step to prevent filter saturation. The process noise for the current step is given by Eq. (12) where Q is the process noise covariance matrix and A is the jacobian of $\boldsymbol{F}$ with respect to the state vector.

$$\dot{S}_{PN} = AS_{PN} + S_{PN}A + Q \tag{12}$$

The state covariance is updated using the Joseph formulation as shown in Eq. (13). The Joseph formulation of the covariance matrix is more consistently symmetric.

$$P_k = \left[I - K_k \tilde{H}_k\right] \bar{P}_k \left[I - K_k \tilde{H}_k\right]^T + K_k R_k K_k^T \tag{13}$$

Consistent with published EKF formulations, the measurement sensitivity matrix $\tilde{H}$ is obtained by taking the partials of the observation with respect to the state vector.

$$\tilde{H} = \left[\frac{\partial \boldsymbol{G}(\boldsymbol{X}, t)}{\partial \boldsymbol{X}}\right]_i^* = \begin{bmatrix} \frac{\partial \mathrm{Az}}{\partial \boldsymbol{X}} \\ \frac{\partial \mathrm{El}}{\partial \boldsymbol{X}} \\ \frac{\partial \rho}{\partial \boldsymbol{X}} \end{bmatrix} \tag{14}$$

where $\boldsymbol{G}(\boldsymbol{X}, t)$ is the current vector of observations and $\boldsymbol{X}$ is the current LROE state.

An important implementation difference in the presented filter used in both estimation loops from the published EKF formulation is the inclusion of a perturbation to the estimated constant state.[35,36] Common between the epoch state filter and the LROE estimation filter is that the estimated state vector is constant. The concern with estimating a constant state vector is that the numerical implementation of the filter is capable of sticking to a particular, and often incorrect, state vector. Therefore, a full state of Gauss-Markov variables are propagated alongside the LROE state vector and are summed onto the LROE state immediately following the time update filter step. This perturbation is achieved from a random sample of a propagated Gauss-Markov process covariance and provides small magnitude alterations. The Gauss-Markov process is initialized from a random sample of the process noise covariance matrix. The Gauss-Markov process is also employed on the spacecraft potential estimate in the filter outer-loop.

The consider covariance addition to the inner filter is achieved by considering the electrostatic potential on each spacecraft. The consider variables are the electorostatic potentials of each craft and are given errors on the order of 5% of the true potential.

$$\boldsymbol{C} = \left[\phi_{\text{obs}},\ \phi_{\text{targ}}\right]^T \qquad \tilde{H}_c = \left[\frac{\partial \boldsymbol{G}(\boldsymbol{X}, t)}{\partial \boldsymbol{C}}\right]_i^* \tag{15}$$

The variation in the state estimate with the inclusion of consider variables is the summation of the EKF state estimate and the consider error, $\boldsymbol{c}$, mapped through the consider sensitivity, M_k.

$$\hat{\boldsymbol{X}}_{ck} = \hat{\boldsymbol{X}}_k + M_k \boldsymbol{c} \tag{16}$$

The truth value of the consider variable $\boldsymbol{c}$ are not known to the inner EKF. Therefore, the filter is initialized with a reasonable guess of the magnitude of this error, is initialized with sufficient covariance, and receives updated consider values from the measurement update of the outer filter. The consider sensitivity M is propagated through each step of the inner filter by

$$\bar{M}_k = \Phi\left(t_k, t_{k-1}\right) M_{k-1} + \theta\left(t_k, t_{k-1}\right) \tag{17a}$$

$$M_k = \left[I - K_k \tilde{H}_k\right] \bar{M}_k - K_k \tilde{H}_{ck} \tag{17b}$$

The evolution of the consider state transition matrix is given by Eq. (18) where A is the jacobian of $\boldsymbol{F}$ with respect to the state vector and Z is the jacobian of $\boldsymbol{F}$ with respect to the consider state vector.

$$\dot{\theta}\left(t, t_k\right) = A\theta\left(t, t_k\right) + Z \tag{18}$$

The presented filter equations compose only the specific instance of the two-time-scale filter. For a complete set of extended Kalman filter and consider covariance equations, refer to Reference.[35]

STATE MEASUREMENT MODELS

The rectilinear filter implementation uses bearing and range measurement models described by

$$\mathrm{Az}_{\text{exact}}(t) = \arctan\left(\frac{y_t(t) - y_o(t)}{x_t(t) - x_o(t)}\right) \tag{19a}$$

$$\mathrm{El}_{\text{exact}}(t) = \arctan\left(\frac{z_t(t) - z_o(t)}{\sqrt{(x_t(t) - x_o(t))^2 + (y_t(t) - y_o(t))^2}}\right) \tag{19b}$$

$$\rho_{\text{exact}}(t) = \sqrt{(x_t(t) - x_o(t))^2 + (y_t(t) - y_o(t))^2 + (z_t(t) - z_o(t))^2} \tag{19c}$$

where the $()_t$ represents the target craft and $()_o$ represents the observer craft. The bearing and range measurements can also be written in terms of the state vector variables by using the mappings provided by Eq. (4) for rectilinear coordinates. The nominal EKF utilizes all azimuth, elevation, and range measurements. The accompanying partial derivatives are included in the Appendix.

The noise for these measurements is applied using a pinhole camera model. Capitalizing on the LROE formulations, the proposed unperturbed filter formulation is an epoch state filter where the current measurement provides information that is mapped to a prescribed epoch. This filter considers the initialization time as the prescribed epoch although the epoch can be altered and reset as necessary. The noise on the measurements is accumulated from two sources. Simulating camera noise, a set of two first order Gauss-Markov variables are propagated and added onto the bearing measurements. In general practice, Gaussian white noise is added to all measurement types. Therefore the measurements provided to the filter are computed by Eq. (20).

$$\mathrm{Az} = \mathrm{Az}_{\text{exact}} + \sigma_{\mathrm{Az}}^{GM} + w_{\mathrm{Az}} \tag{20a}$$

$$\mathrm{El} = \mathrm{El}_{\text{exact}} + \sigma_{\mathrm{El}}^{GM} + w_{\mathrm{El}} \tag{20b}$$

$$\rho = \rho_{\text{exact}} + w_\rho \tag{20c}$$

The inclusion of the Gauss-Markov process more accurately represents the expected performance of a visual navigation camera and the white noise provides the random noise source. The first-order Gauss-Markov random walk process is propagated using the form

$$\dot{\boldsymbol{\sigma}} = -B_{\text{GM}}\boldsymbol{\sigma} + W_k \tag{21}$$

where the B matrix provides the time-constant-drive decay of the current variable value. The white noise process matrix W_k is a randomly sampled value from a camera specific error covariance W. The time constants for the camera considered are 15 minutes such that the Gauss-Markov B matrix is given by

$$B_{\text{GM}} = \begin{bmatrix} 1/\tau_{\mathrm{Az}} & 0 \\ 0 & 1/\tau_{\mathrm{El}} \end{bmatrix} \tag{22}$$

The W matrix is the diagonal covariance of the camera white noise with elements w_{cam}. The camera considered in this study is a 5 mega-pixel, $n_{\text{p}} = 5 \times 10^6$, camera. The noise w_p is assumed to be about 0.05 pixels for 3σ error. The camera is assumed to have a more narrow field of view with a half angle of $\alpha = 10^\circ$. This gives the radian noise magnitude of

$$w_{\text{cam}} = \frac{w_p}{n_{\text{p}}} * 2\alpha \tag{23}$$

The measurement noise for the azimuth and elevation measurements are computed similarly with the range error scaled by the observational baseline.

$$w_{\text{az}} = w_{\text{el}} = \frac{w_m}{n_{\text{p}}} * 2\alpha \tag{24a}$$

$$w_\rho = \rho * \tan\left(\frac{w_r}{n_{\text{p}}} * 2\alpha\right) \tag{24b}$$

where w_m is 0.3 pixels for 3σ error and w_r is 1.5 pixels for 3σ error. These levels of accuracy are possible with modern camera technology and enable the curvilinear formulations. The noise parameters included provide a more realistic benchmark for the LROE EKF formulation.

ILLUSTRATIVE RECTILINEAR LROE ESTIMATION CASES

Of interest is the ability to estimate the relative motion of a target orbital object from a series of space-based observations and the refinement of the target spacecraft potential. The Linearized Relative Orbit Element (LROE) set is well suited to this space-based observation application because the formulation enables reduction of the estimated state space. The LROE extended Kalman filter formulation is implemented in a numerical simulation to demonstrate the feasibility and simplicity of estimating the LROE relative orbit given minimal sensor information. The observations are extracted every 40 seconds from simulated true positions and are then altered by the addition of sensor noise as described in previous sections. The camera noise is defined in Eq. (23) and has a value of 1.56×10^{-5} radians and a nominal range error of 2 centimeters at 200 meter range. To improve filter behavior, a measurement noise under-weighted to 5 times the true noise value as a preliminary filter tuning. The two satellites are inertially propagated with the full nonlinear two-body dynamics and are currently without perturbations. However, additional perturbations are easily included given the LROE dynamics provided by the Lagrangian Brackets.

The target spacecraft is initialized with a semi-major axis of 42160 kilometers and all other orbit elements as zero indicative of a GEO orbit. The true relative orbit is initialized with $\boldsymbol{X}^{\text{true}}$ and the filter is given the initial conditions $\boldsymbol{X}^{\text{true}} + \Delta\boldsymbol{X}$. The LROE filter is applied to a circumnavigating servicer satellite defined by the Cartesian initial conditions and filter state error as

$$\boldsymbol{X}^{\text{true}} = \begin{bmatrix} A_1 \\ A_2 \\ x_{\text{off}} \\ y_{\text{off}} \\ B_1 \\ B_2 \end{bmatrix} = \begin{bmatrix} 0 \\ \text{-}12.5 \\ 0 \\ 0 \\ 0 \\ \text{-}21.66 \end{bmatrix} \text{ [m]} \qquad \Delta\boldsymbol{X} = \begin{bmatrix} 1 \\ 1 \\ 1 \\ 1 \\ 1 \\ 1 \end{bmatrix} \text{ [m]} \tag{25}$$

The electrostatic potential is set to on the order of kilovolts to provide longer observation arcs. The 20 kV magnitudes used for electrostatic detumble evolve much faster than an initialized two-time-scale filter is able to reasonably track. The estimation approach also introduces modeling error

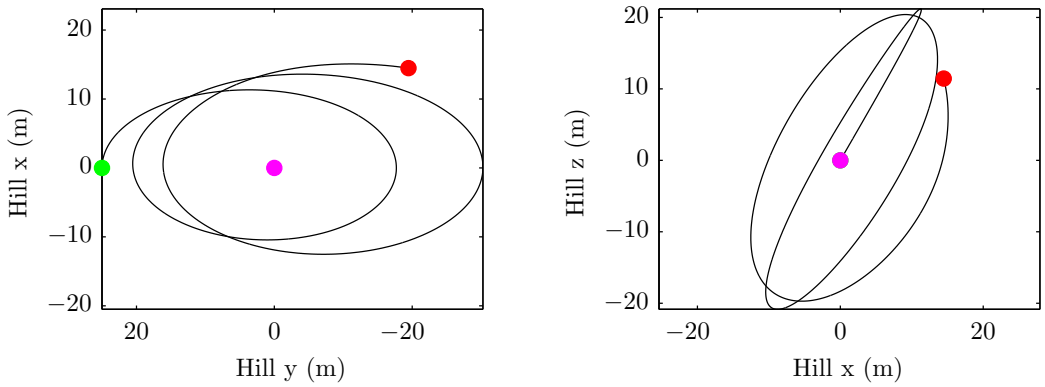

(a) Relative orbit, planar projection.

(b) Relative orbit, XZ projection.

Figure 5. Hill frame relative orbit for the circularly projected example case. Start at o, finish at o about the target.

with the consider errors set to

$$\boldsymbol{C}_{\text{true}} = \left[\phi_{\text{obs}},\ \phi_{\text{targ}}\right]^T = [1900,\ -1700] \qquad \boldsymbol{c} = [10,\ -100] \tag{26}$$

The true drifting relative orbit over a simulated two orbit periods is shown in Cartesian Hill frame coordinates in Figure 5 with the filter cutoff shown in red. The presented Hill frame relative orbit is the basis for the more rapid relative position estimation and the less frequent updates to the target craft potential.

LROE Relative Orbit Estimation

Recall that the CW equations provide the relative motion of a target in Cartesian coordinates as a function of the LROE state. The full LROE state estimation requires bearings and range measurements as required to maintain full rank in the observation sensitivity matrix H. Consider first the case where the full rectilinear state is estimated with bearings and range measurements. In the absence of perturbations, the LROE state is constant and can therefore converge with large initial condition errors. To allow for large initial condition errors the initial filter covariance is exaggerated to $P_0 = 10^{10} \times \text{diag}[1,\ 1,\ 1,\ 1,\ 1,\ 1]$ which also provides ample buffer with the 1 km range of greatest validity inherent in the CW equations. The initial covariance for the consider variables is $P_{cc} = 3\sigma_{V_T}^2 = 3E4$ while the outer filter is initialized with $P_{0,cc} = 100P_{cc}$. The outer filter process 1 out of every 32 inner filter measurements and is delayed 10 inner loop cycles prior to updating the spacecraft electrostatic potential estimate. The inner filter always preserves it's own estimate of the LROE state. The filter process noise, which the LROE state Gauss-Markov is also sampled from, is

$$Q^{\text{est}} = 0.005 \times \text{diag}[1,\ 1,\ 10,\ 10,\ 1,\ 1]$$

The magnitude of the process noise is sufficiently large such that the covariance bounds in the estimate encapsulate the state errors.[37] The process noise term on the x_{off} term is increased to an order of magnitude larger than the terms for other states. This linearization required to obtain the CW equations in the Cartesian frame introduce most of the truncation error into the x_{off} term and so the filter will require greater estimate flexibility in this state variable.

The EKF LROE filter using bearings and range with the initialized state and error detailed in Eq. () achieves a final state error of

$$\boldsymbol{X}_{\text{final}}^{\text{true}} \approx \begin{bmatrix} 0 \\ -12.5 \\ 0 \\ 0 \\ 0 \\ -21.66 \end{bmatrix} \text{(m)} \qquad \boldsymbol{X}_{\text{final}}^{\text{true}} \approx \begin{bmatrix} 14.21 \\ 0.51 \\ 0.90 \\ 6.38 \\ 6.54 \\ -19.42 \end{bmatrix} \text{(m)} \qquad \Delta\boldsymbol{X}_{\text{final}} \approx \begin{bmatrix} 0.137 \\ 0.080 \\ -0.106 \\ -1.869 \\ 0.007 \\ -0.004 \end{bmatrix} \text{(m)}$$

The large LROE state changes caused by the electrostatic interaction over the course of two orbits is well captured with the LROE dynamics in Eq. (6). The estimate errors and 3σ covariance envelopes for each of the LROE states is shown in Figure 6. In an effort to increase filter robustness at the cost of estimation accuracy, he larger covariance on the y_{off} state is in part due to higher process noise on this term for dynamics driven by the x_{off} as well as the electrostatic perturbations. In general, all states are well estimated and the estimation errors are suitable for operational considerations for the electrostatic characterization of the target craft.

The pre- and post-fit residuals for the estimated LROE state are shown in Figure 7. Inspection of the pre-fit residuals reveals the desired trend towards residual noise at the magnitude of the visual sensor capability. The lack of definitive character in the residuals suggests that the state estimate is reasonable and is tending towards an improved target spacecraft potential estimate. The existence of modeling errors in the servicer/observer spacecraft provides that the pre-fit residuals will always demonstrate some character without refinement of the servicer electrostatic potential.

Target Spacecraft Potential Estimation

The target craft electrostatic potential estimation is completed by the outer, slower time scale extended Kalman filter. The outer filter performs one measurement update for every 32 innner loop relative position updates. Furthermore, the propagation of the combined LROE and electrostatic potential state utilizes the inner loop LROE estimate. The outer filter is delayed to allow the inner filter to converge first. The current realization of the filter waits for 10 estimation cycles, or 320 measurements, prior to performing the first update of the electrostatic potential. The start of the estimation and the convergence of the estimate is shown in Figure 8. The final estimate of the target electrostatic potential differs by $\Delta\phi_{\text{tag}} \approx 36.4$ V down from the initialized -100 V error. The present noise model and process noise, convergence of the covariance, and the bias in the servicer potential drive diminishing estimation returns following two orbit periods. However, the filter estimate of the target craft electrostatic potential is comparable to the error injected into the servicer craft potential. This filter demonstrates the feasibility of estimating electrostatic potential from relative motion and advantages of the two-time-scale estimation approach for electrostatic actuation applications.

CONCLUSIONS

The two-time-scale extended Kalman filter architecture is well suited to estimating the electrostatic charge properties of a target craft using only relative position measurements. The two-time-scale approach enables consistent and faster updates to the relative position while still providing enough propagation to significantly capture the target craft electrostatic potential. Such an estimation architecture is valuable because a servicer control law is able to more frequently monitor and correct the relative position which is required for proximity operations. The presented approach is

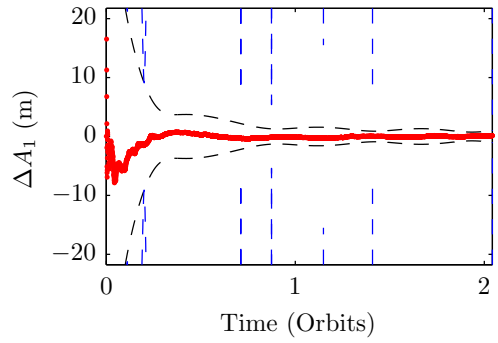

(a) A_1 state and 3σ variance.

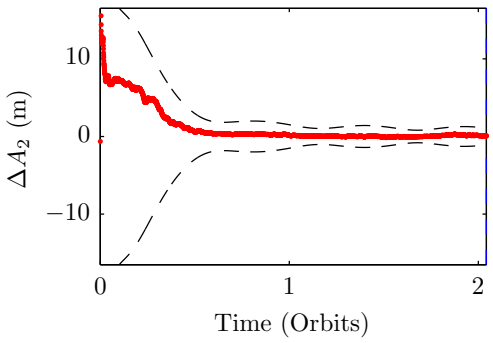

(b) A_2 state and 3σ variance.

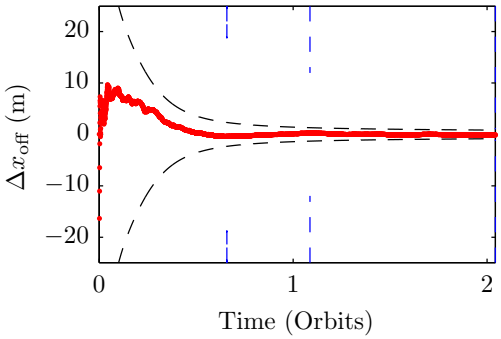

(c) x_{off} state and 3σ variance.

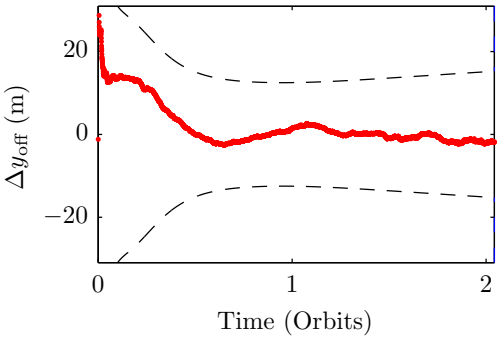

(d) y_{off} state and 3σ variance.

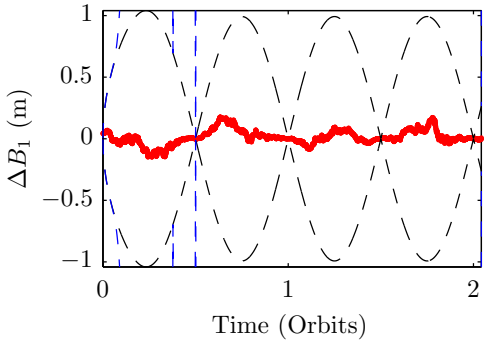

(e) B_1 state and 3σ variance.

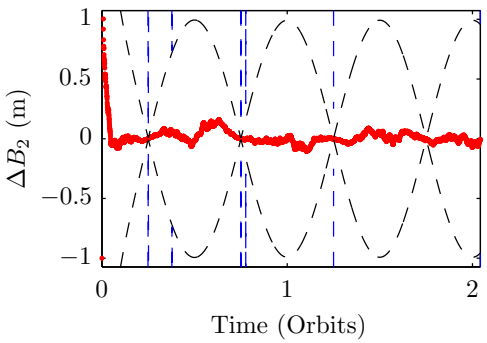

(f) B_2 state and 3σ variance.

Figure 6. LROE estimated state error and covariance envelopes demonstrating full relative motion estimation for LROEs with blue consider covariance envelopes.

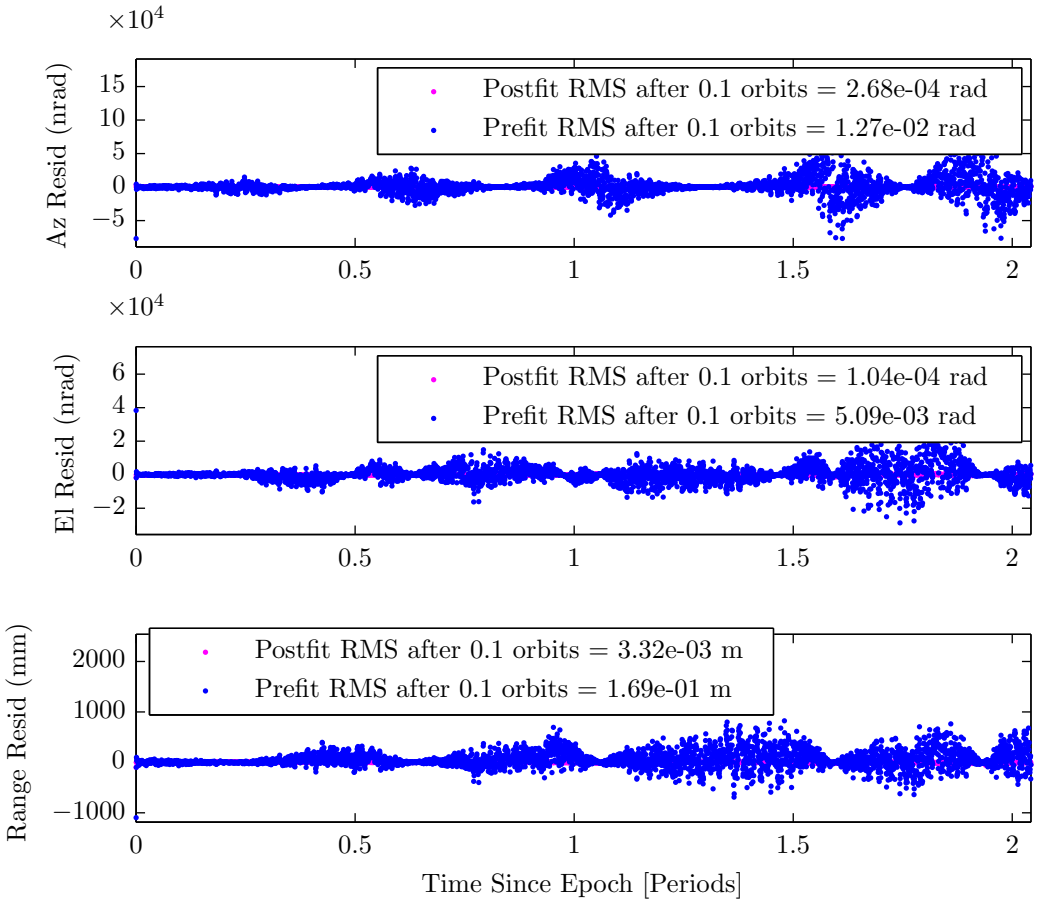

Figure 7. Estimation pre- and post-fit residuals for the full rectilinear LROE set.

well suited for the electrostatic charging characterization of a target craft using the same measurements as used for later detumble and servicing operations. The presented two-time-scale filter also allows for more simple augmentation of the electrostatic estimation where additional measurements and states may be included. Knowledge of the time-varying electrostatic potential on target space objects enables electrostatic actuation for space tug, detumble, and other on-orbit mission concepts.

ACKNOWLEDGEMENTS

The authors would like to thank the NASA Space Technology Research Fellowship (NSTRF) program, grant number NNX14AL62H, for support of this research.

REFERENCES

[1] P. Chrystal, D. McKnight, P. L. Meredith, J. Schmidt, M. Fok, and C. Wetton, "Space Debris: On Collision Course for Insurers?," tech. rep., Swiss Reinsurance Company Ltd, Zürich, Switzerland, March 2011.

[2] P. Couzin, F. Teti, and R. Rembala, "Active Removal of Large Debris: System approach of deorbiting concepts and Technological issues," *6th European Conference on Space Debris*, Darmstadt, Germany, April 22–25 2013. Paper No. 6a.P-17.

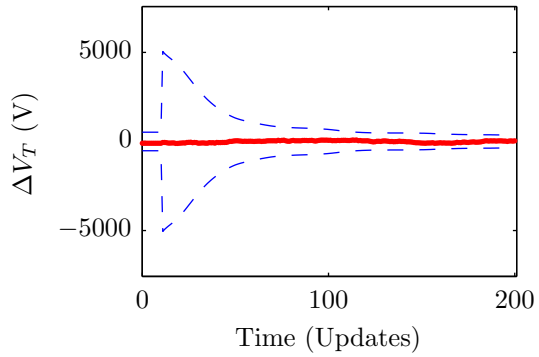

Figure 8. Estimation of the target craft electrostatic potential - updated once for each of 32 LROE state updates.

[3] A. Ogilvie, J. Allport, M. Hannah, and J. Lymer, "Autonomous satellite servicing using the orbital express demonstration manipulator system," *Proc. of the 9th International Symposium on Artificial Intelligence, Robotics and Automation in Space (i-SAIRAS'08)*, Hollywood, CA, February 26-29 2008, pp. 25–29.

[4] W. Xu, B. Liang, B. Li, and Y. Xu, "A universal on-orbit servicing system used in the geostationary orbit," *Advances in Space Research*, Vol. 48, No. 1, 2011, pp. 95–119, 10.1016/j.asr.2011.02.012.

[5] Y. S. Karavaev, R. M. Kopyatkevich, M. N. Mishina, G. S. Mishin, P. G. Papushev, and P. N. Shaburov, "The Dynamic Properties of Rotation and Optical Characteristics of Space Debris at Geostationary Orbit," *Advances in the Astronautical Sciences*, Vol. 119, 2004, pp. 1457–1466. Paper No. AAS-04-192.

[6] A. A. Albuja, D. J. Scheeres, and J. W. McMahon, "Evolution of angular velocity for defunct satellites as a result of YORP: An initial study," *Advances in Space Research*, Vol. 56, July 2015, pp. 237–251, http://dx.doi.org/10.1016/j.asr.2015.04.013.

[7] L. B. King, G. G. Parker, S. Deshmukh, and J.-H. Chong, "Spacecraft Formation-Flying using Inter-Vehicle Coulomb Forces," tech. rep., NASA/NIAC, January 2002. `http://www.niac.usra.edu`.

[8] J. Berryman and H. Schaub, "Analytical Charge Analysis for 2- and 3-Craft Coulomb Formations," *AIAA Journal of Guidance, Control, and Dynamics*, Vol. 30, Nov.–Dec. 2007, pp. 1701–1710.

[9] C. R. Seubert, S. Panosian, and H. Schaub, "Analysis of a Tethered Coulomb Structure Applied to Close Proximity Situational Awareness," *AIAA Journal of Spacecraft and Rockets*, Vol. 49, Nov. – Dec. 2012, pp. 1183–1193.

[10] L. A. Stiles, H. Schaub, K. K. Maute, and D. F. Moorer, "Electrostatically inflated gossamer space structure voltage requirements due to orbital perturbations," *Acta Astronautica*, Vol. 84, Mar.–Apr. 2013, pp. 109–121, 10.1016/j.actaastro.2012.11.007.

[11] S. Wang and H. Schaub, "Nonlinear Charge Control for a Collinear Fixed Shape Three-Craft Equilibrium," *AIAA Journal of Guidance, Control, and Dynamics*, Vol. 34, Mar.–Apr. 2011, pp. 359–366, 10.2514/1.52117.

[12] M. A. Peck, "Prospects and Challenges for Lorentz-Augmented Orbits," *AIAA Guidance, Navigation and Control Conference*, San Francisco, CA, August 15–18 2005. Paper No. AIAA 2005-5995.

[13] B. Streetman and M. A. Peck, "New Synchronous Orbits Using the Geomagentic Lorentz Force," *AIAA Journal of Guidance, Control, and Dynamics*, Vol. 30, Nov.–Dec. 2007, pp. 1677–1690.

[14] H. Schaub and D. F. Moorer, "Geosynchronous Large Debris Reorbiter: Challenges and Prospects," *AAS Kyle T. Alfriend Astrodynamics Symposium*, Monterey, CA, May 17–19 2010. Paper No. AAS 10-311.

[15] D. F. Moorer and H. Schaub, "Hybrid Electrostatic Space Tug," US Patent 0036951-A1, Feb. 17 2011.

[16] D. F. Moorer and H. Schaub, "Electrostatic Spacecraft Reorbiter," US Patent 8,205,838 B2, Feb. 17 2011.

[17] E. Hogan and H. Schaub, "Space Debris Reorbiting Using Electrostatic Actuation," *AAS Guidance and Control Conference*, Breckenridge, CO, Feb. 3–8 2012. Paper AAS 12–016.

[18] N. Murdoch, D. Izzo, C. Bombardelli, I. Carnelli, A. Hilgers, and D. Rodgers, "Electrostatic tractor for near Earth object deflection," *59th International Astronautical Congress*, Glasgow Scotland, 2008. Paper IAC-08-A3.I.5.

[19] N. Murdoch, D. Izzo, C. Bombardelli, I. Carnelli, A. Hilgers, and D. Rodgers, "The Electrostatic Tractor for Asteroid Deflection," *58th International Astronautical Congress*, 2008. Paper IAC-08-A3.I.5.

[20] C. R. Seubert and H. Schaub, "Tethered Coulomb Structures: Prospects and Challenges," *Journal of the Astronautical Sciences*, Vol. 57, Jan.–June 2009, pp. 347–368.

[21] J. H. Cover, W. Knauer, and H. A. Maurer, "Lightweight Reflecting Structures Utilizing Electrostatic Inflation," US Patent 3,546,706, October 1966.

[22] D. Stevenson and H. Schaub, "Multi-Sphere Method for Modeling Electrostatic Forces and Torques," *Advances in Space Research*, Vol. 51, Jan. 2013, pp. 10–20, 10.1016/j.asr.2012.08.014.

[23] E. A. Hogan and H. Schaub, "Impacts of Hot Space Plasma and Ion Beam Emission on Electrostatic Tractor Performance," *IEEE Transactions on Plasma Science*, Vol. 43, Sept. 2014, pp. 3115–3129, 10.1109/TPS.2015.2451001.

[24] T. Bennett and H. Schaub, "Continuous-Time Modeling and Control Using Linearized Relative Orbit Elements," *AAS/AIAA Astrodynamics Specialists Conference*, Vail, CO, August 9-13 2015.

[25] T. Bennett and H. Schaub, "Capitalizing On Relative Motion In Electrostatic Detumbling Of Axi-Symmetric Geo Objects," *6th International Conference on Astrodynamics Tools and Techniques (ICATT)*, Darmstadt, Germany, March 14–17 2016.

[26] T. Bennett and H. Schaub, "Relative Motion Estimation Using Rectilinear and Curvilinear Linearized Relative Orbit Elements," *AAS/AIAA Spaceflight Mechanics Meeting*, Napa Valley, California, Feb. 14–18 2016. Paper No. AAS-16-336.

[27] W. R. Smythe, *Static and Dynamic Electricity*. McGraw–Hill, 3rd ed., 1968.

[28] J. Sliško and R. A. Brito-Orta, "On approximate formulas for the electrostatic force between two conducting spheres," *American Journal of Physics*, Vol. 66, No. 4, 1998, pp. 352–355.

[29] H. Schaub and J. L. Junkins, *Analytical Mechanics of Space Systems*. Reston, VA: AIAA Education Series, 2nd ed., October 2009.

[30] W. H. Clohessy and R. S. Wiltshire, "Terminal Guidance System for Satellite Rendezvous," *Journal of the Aerospace Sciences*, Vol. 27, Sept. 1960, pp. 653–658.

[31] C. Deline, B. E. Gilchrist, C. Dobson, J. E. Jones, and D. G. Chavers, "High accuracy plasma density measurement using hybrid Langmuir probe and microwave interferometer method," *Review of Scientific Instruments*, Vol. 78, 2007, 10.1063/1.2813885.

[32] L. Goembel and J. P. Doering, "Instrument for measuring spacecraft potential," *Journal of Spacecraft and Rockets*, Vol. 35, Jan. – Feb. 1998, pp. 73–81.

[33] L. Goembel, "Measuring Spacecraft Potential with an Electron Spectrometer," *6th Spacecraft Charging Technology Conference*, September 2000.

[34] S. A. R. Hepnar and H. P. Geering, "Adaptive Two-Time-Scale Tracking Filter for Target Acceleration Estimation," *Journal of Guidance*, Vol. 14, No. 3, 1991, pp. 581–588.

[35] B. D. Tapley, B. E. Schutz, and G. H. Born, *Statistical Orbit Determination*. Burlington, MA: Elsevier Academic Press, 2004.

[36] O. Montenbruck, "An epoch state filter for use with analytical orbit models of low earth satellites," *Aerospace Science and Technology*, 2000, pp. 277–287.

[37] T. Bennett and H. Schaub, "Space-to-Space Based Relative Motion Estimation Using Linearized Relative Orbit Elements," Maui, HI, Advanced Maui Optical and Space Surveillance Conference, September 15-18 2015.

APPENDIX

Rectilinear Measurement Sensitivity

The rectilinear azimuth partials are

$$H_{1,1}(t) = \left(-2x(t)\sin(nt) - y(t)\cos(nt)\right)/\kappa_1 \tag{27a}$$
$$H_{1,2}(t) = \left(-2x(t)\cos(nt) + y(t)\sin(nt)\right)/\kappa_1 \tag{27b}$$
$$H_{1,3}(t) = \left(y(t) - \frac{3ntx(t)}{2}\right)/\kappa_1 \tag{27c}$$
$$H_{1,4}(t) = x(t)/\kappa_1 \tag{27d}$$
$$H_{1,5}(t) = 0 \tag{27e}$$
$$H_{1,6}(t) = 0 \tag{27f}$$

where

$$\kappa_1 = x^2(t) + y(t)^2 \tag{28a}$$
$$\kappa_2 = \sqrt{\kappa_1}\left(\kappa_1 + z^2(t)\right) \tag{28b}$$

The rectilinear elevation partials are

$$H_{2,1}(t) = -z(t)\left(2x(t)\cos(nt) - 4y(t)\sin(nt)\right)/2\kappa_1\kappa_2 \tag{29a}$$
$$H_{2,2}(t) = z(t)\left(2x(t)\sin(nt) + 4y(t)\cos(nt)\right)/2\kappa_1\kappa_2 \tag{29b}$$
$$H_{2,3}(t) = \left(-z(t)(2x(t) - nty(t))\right)/2\kappa_1\kappa_2 \tag{29c}$$
$$H_{2,4}(t) = -2z(t)y(t)/2\kappa_1\kappa_2 \tag{29d}$$
$$H_{2,5}(t) = \cos(nt)/\kappa_2 \tag{29e}$$
$$H_{2,6}(t) = -\sin(nt)/\kappa_2 \tag{29f}$$

The rectilinear range partials are

$$H_{3,1}(t) = \left(x(t)\cos(nt) - 2y(t)\sin(nt)\right)/2\rho \tag{30a}$$
$$H_{3,2}(t) = \left(-x(t)\sin(nt) - 2y(t)\cos(nt)\right)/2\rho \tag{30b}$$
$$H_{3,3}(t) = \left(2x(t) - 3nty(t)\right)/2\rho \tag{30c}$$
$$H_{3,4}(t) = y(t)/\rho \tag{30d}$$
$$H_{3,5}(t) = z(t)\cos(nt)/\rho \tag{30e}$$
$$H_{3,6}(t) = -z(t)\sin(nt)/\rho \tag{30f}$$
$$\tag{30g}$$